Polarization-resolved photoluminescence study of an atom probe tip containing a ZnO-(Mg,Zn)O heterostructure

Pradip Dalapati, Eric Weikum, Georges Beainy, Enrico Di Russo, Jonathan Houard, Simona Moldovan, Angela Vella, Jean Michel Chauveau, Maxime Hugues, Nolwenn Le Biavan, et al.

Polarization-resolved photoluminescence study of an atom probe tip containing a ZnO-(Mg,Zn)O heterostructure

P. Dalapati[a,b], E. M. Weikum[a], G. Beainy[a], E. Di Russo[a], J. Houard[a], S. Moldovan[a], A. Vella[a], J.M. Chauveau[c,d], M. Hugues[c], N. Le Biavan[c], M. Tchernycheva[e], F.H. Julien[e], Z. Saghi[f], L. Rigutti[a]*.

[a] UNIROUEN, CNRS, Groupe de Physique des Matériaux, Normandie Université, 76000 Rouen, France; [b] Research Center for Nano-Devices and Advanced Materials, Nagoya Institute of Technology, Nagoya 466-8555, Japan; [c] Université Côte d'Azur, CNRS, CRHEA, 06560 Valbonne, France, [d] Groupe d'Etude de la Matière Condensée, UMR 8635 CNRS, Université Versailles St Quentin/Paris Saclay. 78000 Versailles, France; [e] Centre de Nanosciences et de Nanotechnologies, CNRS UMR 9001, Univ. Paris-Sud, Université Paris-Saclay, C2N – Orsay, 91405 Orsay Cedex, France; [f] Univ. Grenoble Alpes, CEA, Leti, Grenoble F-38000, France

*lorenzo.rigutti@univ-rouen.fr

ABSTRACT

We studied polarization-resolved photoluminescence originating from a ZnO-(Mg,Zn)O quantum well heterostucture embedded within an atom probe tip, i.e. a nanoscale needle-shaped sample with apex radius of several tens of nm, prepared by focused ion beam. The study was carried out within a photonic atom probe before the atom probe analysis of the sample. This setup allows for the analysis of the polarization of the photoluminescence emitted by the tip and for its orientation around its axis. While the photoluminescence emitted by bulk ZnO and by the (Mg,Zn)O alloy is strongly polarized along the tip axis, coinciding with the crystal [1-100] axis, the ZnO/(Mg,Zn)O quantum well luminescence appears to be strongly polarized along its in-plane direction, perpendicular to the crystal [1-100] axis. Finite-difference time domain calculations provide a key for the interpretation of these results in terms of selection rules and of effects related to the waveguide effect of the tip.

Keywords: Photoluminescence, polarization, oxides, heterostructures, quantum well, atom probe tomography, nanoscale sample.

1. INTRODUCTION

Polarization-resolved photoluminescence (PL) and micro-photoluminescence (µPL) yields important information for the study of the optical properties of solids. The light emitted by radiative dipoles embedded in solids can be characterized by specific polarization properties that depend on the selection rules of the dipole itself (these, in turn, depend on factors such as the symmetry of the system or the overlap of electronic wavefunctions involved in the transition) but may also depend on the specific shape of the emitting system via the contrast between the refractive indexes of the emitting and of the surrounding medium. This interplay between intrinsic selection rules and system morphology has been previously highlighted in studies on the polarization properties of nanowires: as an example, very thin nanowires tend to emit light polarized along their main axis (π-polarization) unless a selection rule, which may be typical of crystal structures, defects or quantum emitters, forces a polarization perpendicular to the axis (σ-polarization) [1,2]. The interest for the study of polarization-resolved PL from nanoscale systems is not limited to nanowires: it has become recently possible to isolate a few or even single quantum-confined light emitters within nanoscale objects realized with a top-down approach, as in the case of lamellas or field-emission tips obtained by focused ion beam (FIB). These structures have a particular interest in correlative microscopy, as they open up the possibility to study the same system by optical spectroscopy (PL[3–5] or cathodoluminescence[6], spatial modulated spectroscopy[7], etc.) and by microscopy technique with atomic or nearly-atomic spatial resolution, such as transmission electron microscopy (TEM) or atom probe tomography (APT). The correlative analysis may be conducted ex-situ, through a sequential approach[3], or even in-situ, as in the case of a CL-equipped TEM or in the recently demonstrated Photonic Atom Probe (PAP)[8,9]. This work is related to this last technique, as it exploits the PAP environment in order to study polarization-resolved µPL from nanoscale tips containing a ZnO-(Mg,Zn)O

heterostucture. This last structure has been previously studied by a PAP approach, revealing the optical signatures of the strain induced by the electric field applied to the tip apex in order to promote ion evaporation[10]. However, these previous studies did not consider the information carried by the polarization of the emitted light. This issue is addressed in this work focusing on the main spectral components of the PL spectra, i.e. the emission from the ZnO substrate, from the (Mg,Zn)O alloy and, in particular, from the ZnO quantum well.

2. EXPERIMENTAL DETAILS

2.1 Analyzed structure

The studied structure is a double ZnO/(Mg,Zn)O quantum well system grown on a non-polar wurtzite (WZ) m-plane ZnO substrate by plasma assisted molecular beam epitaxy (PA-MBE), as further detailed in Ref. [5,11,12]. The thickness of the different layers and the alloy composition of the (Mg,Zn)O barriers were designed in order to avoid plastic relaxation. The structure is visualized in two different orientations in the electron tomography (ET) images reported in Fig. 1-(a). The two QW have been numbered here in the order of their growth. Their thicknesses are t_1 = (2.0±0.1) nm and t_2 = (3.9±0.1), respectively. Notice that, as TEM performed at 200 keV may damage the sample introducing non-radiative recombination centers, the tip specimen reported in Fig. 1-(a) is not one of those analyzed by PAP and by polarization-resolved µPL. The substrate-alloy interface and the QW interfaces are clearly marked by a serrated profile, a morphological feature propagating throughout the epitaxial growth of the structure [5]. This profile has been found to be related to compositional inhomogeneities within the barriers, with the formation of Zn- and Mg- enriched regions corresponding to the edges pointing towards the substrate and towards the upper surface, respectively. This feature, along with the QW interface profile, is visible in both the top ET image, oriented along the [0001] crystal axis, and on the composition map extracted from APT analysis and reported in Fig. 1-(b). The mechanism leading to such features and its effect on the electronic properties of the system have been discussed in previous works [5,10]. According to APT results, the average Mg site fraction, is $\langle x_{Mg} \rangle$=0.27.

The tip-shaped field emitters were prepared by FIB in a ZEISS Nvision40 SEM-FIB dual beam system. The preparation was carried out by standard lift-out and milling using and acceleration voltage of 30 kV for the Ga ions during sample milling, with a final cleaning step at 2 kV. This protocol is designed to preserve the PL signal from the QW#1 and from the (Mg,Zn)O barriers, while the signal of QW#2 (closer to the tip apex) is barely or non- detectable for different specimens, as quenched by the damage introduced by the Ga ions. The tip specimen studied in this work is reported in the scanning electron micrograph of in Fig. 1-(c). Consistent results were obtained from four different tip specimens.

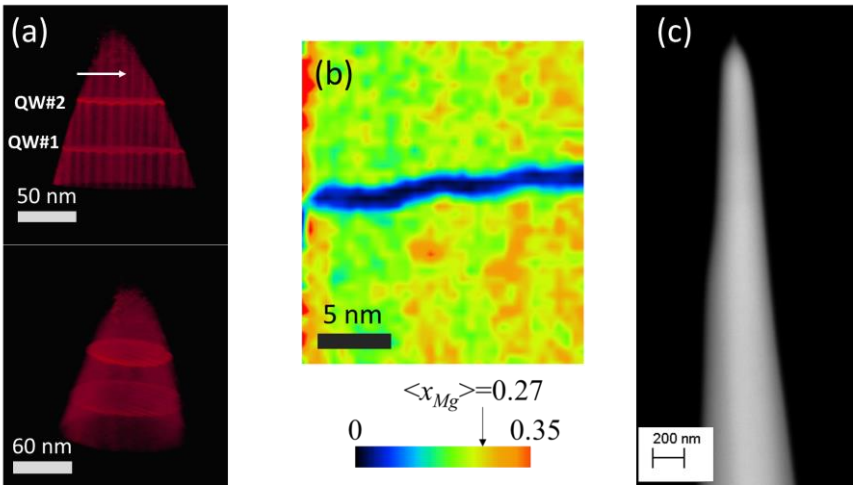

Figure 1. The system under study. (a) Electron tomography image of a tip apex containing the ZnO/(Mg,Zn)O heterostructure; (b) Mg site fraction map issued from atom probe tomography analysis of the tip. The fraction map refers to a 2 nm thick slice containing the QW#1; (c) Scanning electron micrograph of the tip studied in this work, as prepared by focused ion beam.

2.2 Experimental setup

A schematic of the experimental setup is reported in Fig. 2-(a). The tip is analyzed within the photonic atom probe (PAP) described in detail in ref.[8]. In this work, this instrument is used for PL measurement only. A pulsed laser beam (pulse duration ~150 fs, frequency 4 MHz, wavelength 266 nm) is focused onto the tip by a parabolic mirror. The beam waist at the focal point has been estimated to be of the order of one to two micron. The beam illuminates thus the whole heterostructure region and a part of the ZnO substrate, which is much larger than the illuminated region. A fraction of the PL produced by the sample is collected through the same optical path, which is used to focus the fs-laser on the tip's apex. The angular aperture of the mirror, given by the system's smallest aperture (exit pupil) is ϑ_{max} = 20°, roughly corresponding to 4% of the solid angle. The light is then directed towards the spectrometer, where it is dispersed by a 600 lines/mm grating and recorded by a CCD array, with a spectral resolution of 0.1 nm[8]. Prior to injection in the spectrometer, the light passes through a linear polarizer designed for filtering light in the interval 300-400 nm.

As illustrated in Fig. 2-(b), all prepared tips have the axis oriented along the [1-100] direction (m-direction) of the WZ crystal, with a possible misalignment of ±5°. The tip axis also corresponds to the *x*-axis of the instrument reference system, while the *z*-axis corresponds to the optical axis. Polar angles ϑ and φ can also be defined in order to describe the far field propagation of the light beam. As a practical aspect of this setup, the tip can be rotated around its axis, so that either the [11-20] direction (crystal a-direction) or the [0001] direction (the polar c-direction) can be aligned with the optical axis. Intermediate tip orientations, where the optical axis takes the direction of a linear combination of a and c can obviously also be selected, but only a and c-oriented tips were studied. All PL spectra have been collected after stabilizing the sample temperature at T=50K.

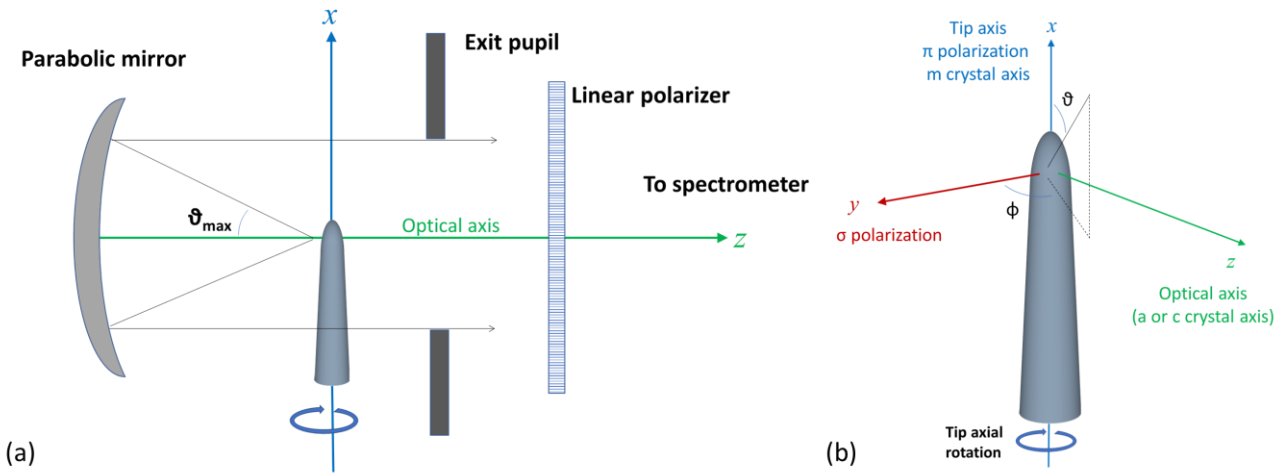

Figure 2. (a) Schematic of the experimental setup – the parabolic mirror lies inside the atom probe chamber (not shown); (b) Reference frame showing the main axes and the polar and azimuthal angles, along with the two main polarization directions; the orientation of the tip can be varied by rotating it around its main axis, coinciding with the crystal m-axis ([1-100] direction).

3. EXPERIMENTAL RESULTS

Unpolarized and polarization-resolved spectra have been collected for two tip orientations, i.e., with the a-axis and with the c-axis of the crystal parallel to the optical axis z. Polarized spectra were collected by varying the polarizer angle by steps of 10°. Within the polarizer reference frame, 0° corresponds to the electric field polarized along the tip axis, i.e. to

π-polarization, while 90° corresponds to σ-polarization. Figure 3 reposts the results of the optical spectroscopy study. Selected PL spectra from the tip with the a-axis oriented along the optical axis (in the following, we will refer to this configuration as to the "a-oriented tip", while the alternative configuration will be referred to as the "c-oriented tip") are displayed in Fig. 3-(a). For the same integration time (60s) the unpolarized spectrum is, as expected, around one order of magnitude more intense than the filtered spectra. The decrease of PL intensity upon polarization filtering is the main reason why an analysis of the entire tip's evaporation process as shown in ref. [10] was not performed in a polarization filtered manner. The required illumination time would increase the time required for the PAP measurement by an order of magnitude. Three main spectral contributions can be recognized, the assignments having been discussed in previous works [9,10]: the (Mg,Zn)O barrier exhibits a broad emission peaked at the energy E=3.9 eV, the QW#1 has a narrower peak at E=3.47 eV, while the ZnO substrate is peaked at E=3.38 eV and displays a sub-bandgap structure which is partly related to phonon replicas. The polar diagrams of the a-oriented tip, reporting the dependence of the intensity of each spectral component (normalized to its maximum) on the polarizer angle, are shown in Fig. 3-(b), and clearly point out that the ZnO substrate and the (Mg,Zn)O barrier emit moderately π-polarized light, while the QW is moderately σ-polarized. The polarization ratios, defined for each spectral component as $P=(I_\sigma - I_\pi)/(I_\sigma + I_\pi)$, are reported in Table 1. The intensities I_σ and I_π are determined on the basis of the cosine square fit of each polar diagram.

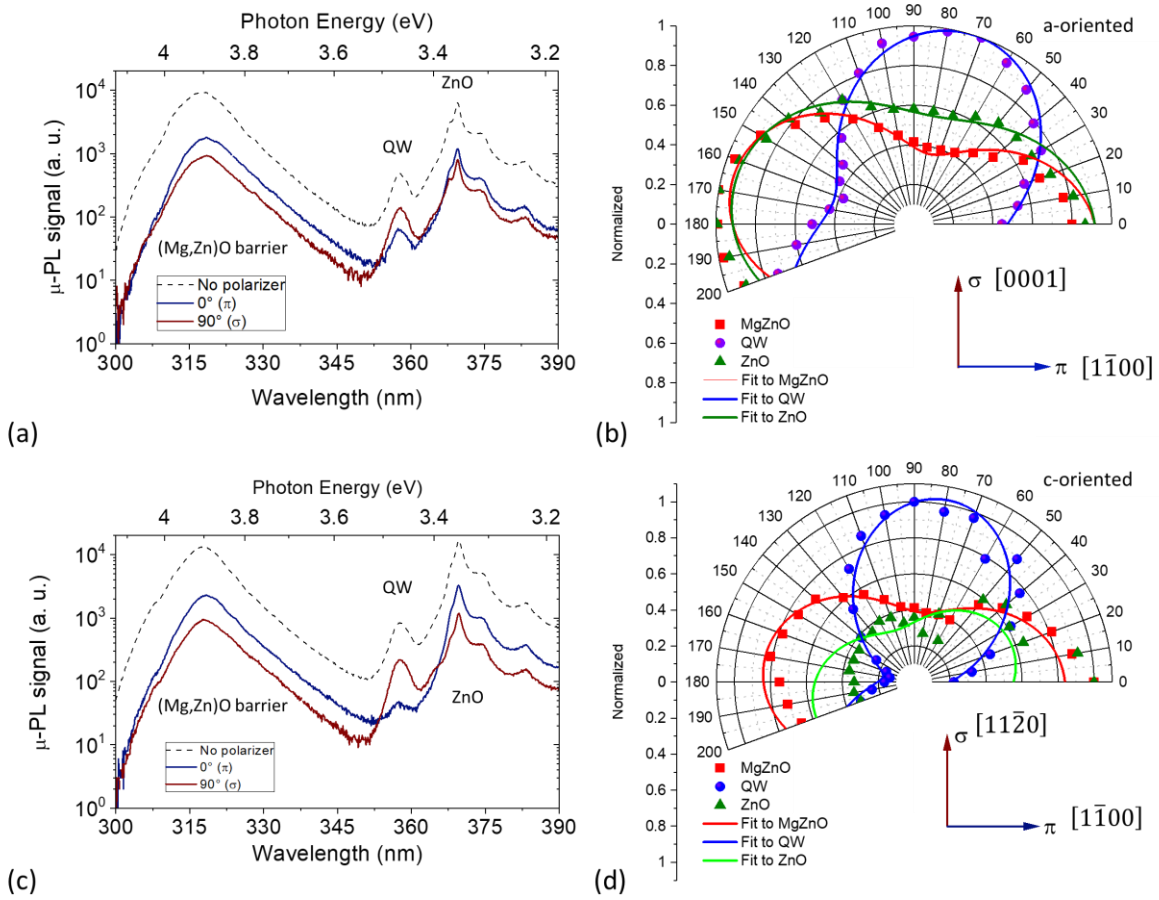

Figure 3. Polarization-resolved PL from the atom probe tip: (a) Unpolarized and selected polarized PL spectra from the tip and (b) polarization diagram from the three main spectral components ((MgZn)O barrier, QW#1 and ZnO substrate) when the optical axis corresponds to the crystal a-axis ([11-20] direction). (c) Unpolarized and selected polarized PL spectra from the tip and (d) polarization diagram from the three main spectral components when the optical axis corresponds to the crystal c-axis ([0001] direction).

The results of the measurements performed on the c-oriented tip are displayed in Fig. 3-(c,d). The polarization behavior of the three spectral components is similar to that recoded for the a-orientation, with the main difference that the QW signal becomes here strongly σ-polarized (P_{QW}=0.76).Table 1. Polarization ratios ($P=(I_\sigma - I_\pi)/(I_\sigma + I_\pi)$) for the different spectral components and tip orientations.

Table 1. Polarization ratios for the different spectral components and tip orientations.

		Spectral component		
		ZnO (3.38 eV)	**QW#1 (3.47 eV)**	**(Mg,Zn)O (3.9 eV)**
Tip orientation	**a-oriented**	-0.27	0.45	-0.44
	c-oriented	-0.58	0.76	-0.36

4. CALCULATION OF POLARIZATION-RESOLVED FAR FIELD PATTERNS

The studied system differs significantly from a dipole emitting in an isotropic medium. In order to correctly interpret the measured polarization patterns and ratios, we have performed finite difference time domain (FDTD) calculations of the emission patterns of three main dipole orientations, as illustrated in the first column of Fig. 4, corresponding to a dipole oriented along the *x*-axis (tip axis, m-direction), along the *y*-axis and along the *z*-axis (optical axis).

4.1 Calculation methods

The simulation space is defined according to the microscopy data (TEM, SEM and APT). The refractive index of ZnO is extracted from ref. [13], while for (Mg,Zn)O, due to the lack of data for this specific alloy composition and compositional inhomogeneity, we blue-shifted the refractive index of ZnO by a quantity equal to the difference in the PL energy of the (Mg,Zn)O and ZnO peaks and treated (Mg,Zn)O as a homogeneous medium. The dipole emission source is placed in the center of the quantum well and emits with a peak energy equal to that of the QW PL. The quantum well's refractive indexes were considered to be the same as of bulk ZnO. This is a good approximation for the study of the localized emission from QW#1. We limited our calculation to this case due to *(i)* the much higher computational charge that would be required in order to calculate non-localized emission from the much larger regions containing ZnO or (Mg,Zn)O and *(ii)* the fact that the distribution of these dipoles is a priori unknown. Within the Lumerical framework the far-field Poynting vector was calculated, weighted with the solid angle $d\Omega = \sin\vartheta \bullet d\vartheta \bullet d\varphi$ and finally used in order to generate the emission maps shown in the second column of Fig. 4, which show the emitted power as a function of the spherical angles. Furthermore, for each emission angle we took the effect of a reflection on an infinitely extended parabolic mirror on the light's polarization into account in order to generate intensity maps corresponding to either π- or σ-polarized light for each dipole orientations, as reported in the third and fourth columns of Fig. 4. Notice that obviously only part of the emitted light propagates within the field of view of the mirror-exit pupil system. This set of angles is highlighted in the emission patterns through the black circle, and the intensity lying within the circle contributes to the calculation of the detection yield – i.e. of the ratio between the intensity coupled into the spectrometer and the total emitted intensity – and of the polarization ratios; these values, which clearly depend on the system configuration, are reported in Table 2. Finally, we verified that the effect of the anisotropy of the refractive index typical of the WZ crystal has no significant effect on the emission patterns of all dipole orientations.

4.2 Behavior of the main dipole orientations of QW#1

The results of the calculations for the *x*-oriented dipole emission from QW#1 are displayed in Fig. 4-(a). As expected, the emission pattern is invariant with respect to the rotation around the tip axis. The yield of the detection system, reported in Table 2, is around 3.96 % for the π-polarized light, and negligible for the σ-polarized light, resulting in a polarization ratio of around -1. A different picture results from the y-oriented dipole, as in Fig. 4-(b). The yield for this dipole is 3.46 % and the detected light is almost exclusively σ-polarized, with a polarization ratio close to 1. An intermediate situation concerns the dipole oriented along the optical axis, presented in Fig. 4-(c). As a result of system anisotropy, there is significant light coupling into the spectrometer, with a total yield (σ+π polarizations) of 1.4 %, comparable to that of the

dipoles oriented perpendicularly to the optical axis. Although the light coupled into the spectrometer is mostly π-polarized, a weaker but significant portion of σ-polarized light is also detected, yielding a polarization ratio of -0.87. These facts should be considered when analyzing experimental polarization patterns, as they indicate that the polarization of the light may be significantly influenced by a radiating dipole oriented along the optical axis.

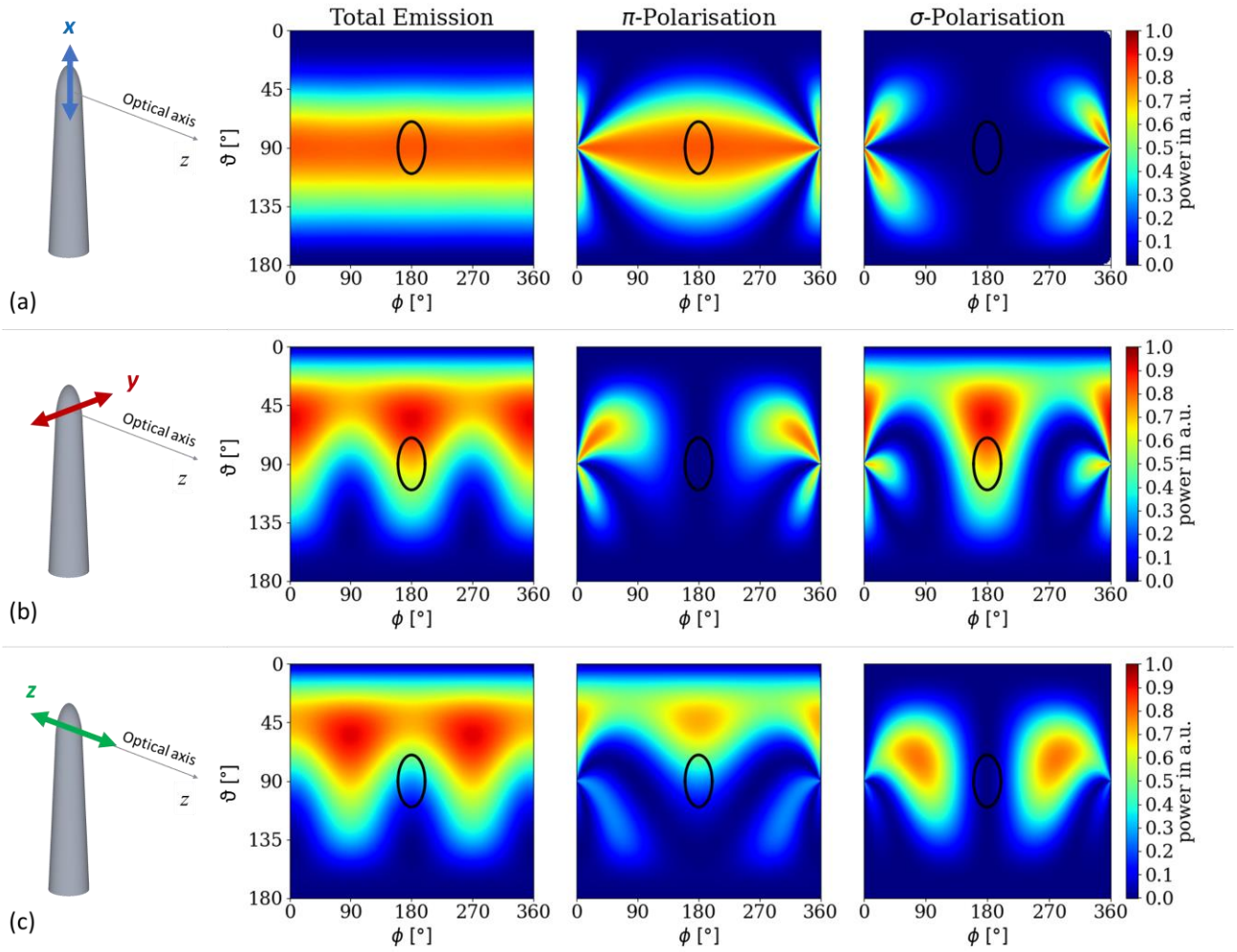

Figure 4. Finite-difference time domain (FDTD) calculations showing the three main dipole orientations (first column) and the emitted radiation patterns: total emission (second column), emission detected as π-polarized (third column) and emission detected as σ-polarized (fourth column). Line (a) refers to a dipole oriented along the x-axis (crystal m-axis, tip axis), line (b) to a dipole oriented along the y-axis, while line (c) to a dipole oriented along the optical axis. The black circle superimposed to the emission patterns corresponds to the field of view of the spectrometer, as illustrated in figure 2.

Table 2. Calculated yields in % and polarization ratios for the three main dipole orientations.

		Dipole orientation		
		x	*y*	*z*
Yields (%)	σ – polarization	0.0006	3.41	0.097
	π - polarization	3.93	0.038	1.36
Polarization Ratio		-0.9997	0.98	-0.87

5. DISCUSSION

The experimental results and the FDTD calculations allow us drawing several conclusions on the optical properties of the studied sample. The main experimental results point out that the polarization of the ZnO and (Mg,Zn)O emission is moderately oriented along the tip axis, while the QW emission is more strongly polarized perpendicularly to the tip axis, i.e. in the QW plane.

5.1 ZnO substrate

According to past studies[14], the ZnO-substrate's signal should appear as strongly polarized perpendicularly to the c-axis. This would imply a high degree of π-polarization with the tip in the a-orientation and a significantly lower degree of π-polarization with the tip in the c-orientation. The experimental results, on the contrary, display a moderate π-polarization in both orientations. This is most likely due to the morphology of the tip (we remind that the simulation of the ZnO substrate does not fall within the scope of our calculations) and to its waveguide effect, which could significantly mix different polarization components from an extended distribution of emitting dipoles.

5.2 (Mg,Zn)O barrier

A similar situation is found in the case of the (Mg,Zn)O-barrier emission. It is interesting to notice that a previous study of the polarization dependence the absorption edges of m-plane (Mg,Zn)O layers indicates that the lower-energy absorption edge is perpendicular to the c-axis for $x_{Mg}<0.24$, then the polarization is inverted and for higher Mg content the lower-energy absorption edge is parallel to the c-axis[15]. The data from this work indicate a polarization behavior similar to the ZnO. Care should be taken when comparing the two emissions because they are not localized within the same portion of the tip. However, the (Mg,Zn)O emission is more strongly π-polarized when the tip is a-oriented, which suggests a weaker emission from c-oriented dipoles. This is in agreement with past works, as we can notice that the average content of the (Mg,Zn)O alloy is $x_{Mg}=0.27$, but it is highly inhomogeneous, and it is reasonable to expect that most optical transitions will be due to carriers localized within regions with $x_{Mg}<0.27$.

5.3 ZnO/(Mg,Zn)O quantum well

Most interestingly, the QW#1 emission is polarized perpendicularly to the tip axis, and this σ-polarization is stronger when the tip is c-oriented. Previous works on the polarization of the PL emitted from thin films containing m-plane ZnO/(Mg,Zn)O quantum wells reported that the PL is strongly polarized perpendicular to the c-axis[16]. The results of our experimental work differ from those of ref. [16]. On one hand, the polarization along m appears to be suppressed for the QW PL. On the other hand, when the tip is a-oriented (crystal a-direction along the optical axis) the light is σ-polarized, i.e. polarized along c, which contradicts the results of ref. [16] If a certain amount of light from an a-oriented dipole could still couple into the detector, as suggested by the FDTD calculations, it should nevertheless inject in it mostly π-polarized light. This leads us to conclude that the QW#1 PL is mostly polarized within the m-plane. The reason why this occurs is not completely clarified, but some hypotheses can be discussed. It is unlikely that the unusual polarization behavior of QW#1 is driven by the strain relaxation of the barrier. The (Mg,Zn)O alloy is indeed grown as a thin film epitaxially strained on the ZnO substrate. Under these conditions, the QW#1 is unstrained. When a tip is fabricated by FIB, the strain in the heterostructure can partly relax at lateral surfaces, producing in inhomogeneous strain state within the barrier and the QW. The maximum strain state within the QW has been evaluated in a previous work[10] as $\varepsilon_{aa} \sim 0.3\%$ and $\varepsilon_{cc} \sim -0.4\%$. Under these conditions, the ZnO valence band states retain about 93% of the character of the unstrained ZnO. Further admixture among valence band states could be originated by quantum confinement and by the mixing with (Mg,Zn)O states. However, this would not explain why the polarization behavior of this system differs from that of ref [16]. A further possibility is related to the specific morphology of the quantum well, which is known to produce strong carrier localization effects and could thus lead to further mechanisms of band mixing. It is interesting to notice that this specific morphology is at the origin of the intersubband absorption of infrared light with the electric field parallel to the m-plane[17]. The intersubband absorption mechanism is obviously different from the interband emission treated here, but underlines the importance of QW morphology for optical transitions.

6. CONCLUSIONS AND PERSPECTIVES

In summary, we have conducted a study of the polarization properties of the PL emitted by a ZnO/(Mg,Zn)O-quantum well heterostructure embedded in nanoscale tip fabricated by FIB and analyzable by atom probe tomography. As a

peculiar feature of this system, it is straightforward to control the orientation of the tip along its axis, and it becomes thus possible to select specific crystal directions to be parallel or perpendicular to the optical axis. As the analyzed system has not a standard morphology such as that of a thin film or of a thin nanowire, FDTD calculations were carried out in order to predict the amount of detected light and its polarization for three main orientations of a dipole emitting at the center of the QW.

6.1 Polarization behavior of the PL from the ZnO/(Mg,Zn)O heterostructure

The measurements conducted on several tips and here reported for one of them indicate that the ZnO and (Mg,Zn)O PL spectral contributions are moderately polarized along the tip axis, which is in reasonable agreement with previous studies on thin films or on nanowires. On the other hand, the QW PL exhibits a σ-like polarization that points out to the presence of radiative dipoles both in the a- and in the c-direction of the crystal. This result disagrees with previous studies. A tentative explanation of this situation should consider the specific QW morphology and the mechanisms of carrier localization that it induces.

6.2 Polarization-resolved PAP

The study of polarization-resolved PL within a PAP is an original experimental method which the development of this instrument has recently made possible. Among its advantages we can identify the possibility of orient the tip in order to obtain complementary information about the polarization behavior with respect to different sets of crystal axes. However, we have also shown that the interpretation of such information is not straightforward, as the radiation patterns and the polarization of the detected light are strongly influenced by the tip morphology and composition. Another interesting point is the possibility to orient the tip preliminarily to APT analysis, in order to obtain the highest PL signal or the highest polarization ratio for a given spectral component. The acquisition of polarization-resolved PL in-situ and operando during the APT analysis, within the PAP framework, is possible, provided the attenuation of the PL signal by the polarizing filter does not hinder the acquisition of PL spectra with a correct signal-to-noise ratio.

REFERENCES

1. H. E. Ruda and A. Shik, “Polarization-sensitive optical phenomena in semiconducting and metallic nanowires,” Phys. Rev. B **72**(11), 115308 (2005) [doi:10.1103/PhysRevB.72.115308].
2. L. Rigutti et al., “Photoluminescence polarization properties of single GaN nanowires containing GaN/AlGaN quantum discs,” Phys. Rev. B **81**(4), 045411 (2010) [doi:10.1103/PhysRevB.81.045411].
3. L. Rigutti et al., “Correlation of Microphotoluminescence Spectroscopy, Scanning Transmission Electron Microscopy, and Atom Probe Tomography on a Single Nano-object Containing an InGaN/GaN Multiquantum Well System,” Nano Lett. **14**(1), 107–114 (2014) [doi:10.1021/nl4034768].
4. L. Mancini et al., “Multi-microscopy study of the influence of stacking faults and three-dimensional In distribution on the optical properties of m-plane InGaN quantum wells grown on microwire sidewalls,” Applied Physics Letters **108**(4), 042102 (2016) [doi:10.1063/1.4940748].
5. E. Di Russo et al., “Three-dimensional atomic-scale investigation of ZnO-MgxZn1−xO m-plane heterostructures,” Appl. Phys. Lett. **111**(3), 032108 (2017) [doi:10.1063/1.4994659].
6. G. Schmidt et al., “Direct evidence of single quantum dot emission from GaN islands formed at threading dislocations using nanoscale cathodoluminescence: A source of single photons in the ultraviolet,” Applied Physics Letters **106**, 252101 (2015) [doi:10.1063/1.4922919].
7. A. Vella et al., “Optothermal response of a single silicon nanotip,” Phys. Rev. B **97**(7), 075409, American Physical Society (2018) [doi:10.1103/PhysRevB.97.075409].
8. J. Houard et al., “A photonic atom probe coupling 3D atomic scale analysis with in situ photoluminescence spectroscopy,” Review of Scientific Instruments **91**(8), 083704, American Institute of Physics (2020) [doi:10.1063/5.0012359].
9. E. Di Russo et al., “Super-resolution Optical Spectroscopy of Nanoscale Emitters within a Photonic Atom Probe,” Nano Lett. **20**(12), 8733–8738, American Chemical Society (2020) [doi:10.1021/acs.nanolett.0c03584].

10. P. Dalapati et al., “In Situ Spectroscopic Study of the Optomechanical Properties of Evaporating Field Ion Emitters,” Phys. Rev. Applied **15**(2), 024014, American Physical Society (2021) [doi:10.1103/PhysRevApplied.15.024014].
11. J.-M. Chauveau et al., “Benefits of homoepitaxy on the properties of nonpolar (Zn,Mg)O/ZnO quantum wells on a-plane ZnO substrates,” Appl. Phys. Lett. **97**(8), 081903 (2010) [doi:10.1063/1.3481078].
12. J.-M. Chauveau et al., “Non-polara-plane ZnMgO1/ZnO quantum wells grown by molecular beam epitaxy,” Semicond. Sci. Technol. **23**(3), 035005 (2008) [doi:10.1088/0268-1242/23/3/035005].
13. H. Y. H. Yoshikawa and S. A. S. Adachi, “Optical Constants of ZnO,” Jpn. J. Appl. Phys. **36**(10R), 6237, IOP Publishing (1997) [doi:10.1143/JJAP.36.6237].
14. G. Jacopin et al., “High degree of polarization of the near-band-edge photoluminescence in ZnO nanowires,” Nanoscale Research Letters **6**(1), 501 (2011) [doi:10.1186/1556-276X-6-501].
15. M. D. Neumann et al., “Inversion of absorption anisotropy and bowing of crystal field splitting in wurtzite MgZnO,” Appl. Phys. Lett. **108**(22), 221105, American Institute of Physics (2016) [doi:10.1063/1.4953159].
16. H. Matsui and H. Tabata, “In-plane anisotropy of polarized photoluminescence in M-plane ($10\bar{1}0$) ZnO and MgZnO/ZnO multiple quantum wells,” Appl. Phys. Lett. **94**(16), 161907, American Institute of Physics (2009) [doi:10.1063/1.3124243].
17. M. M. Bajo et al., “Intersubband absorption at normal incidence by m-plane ZnO/MgZnO quantum wells,” in Oxide-based Materials and Devices X **10919**, pp. 212–217, SPIE (2019) [doi:10.1117/12.2509524].

ACKNOWLEDGEMENTS

This work was funded by the French National Research Agency (ANR) in the framework of the projects EMC3 Labex IDEPOP and ANR-13-JS10-0001-01 TAPOTER and co-funded in the framework of RIN IFROST, EMC3 Labex IDEPOP and CPER CATHY-2 projects by European Union with European Regional Development Fund (ERDF) and by Region Normandie. The authors from CRHEA and C2N also acknowledge funding from the EU Commission Horizon 2020 through the ZOTERAC project.